Memory effect in the plasticity of a silicate glass densified at room temperature

T. Deschamps[1], C. Martinet,[1] B. Champagnon,[1] G. Molnár[2], and E. Barthel[3]

[1]*Institut Lumière Matière, UMR 5306 Université Lyon1-CNRS, Université de Lyon 69622 Villeurbanne, France*
[2]*Université Lyon, CNRS, INSA Lyon, LaMCoS, UMR5259, 69621 Villeurbanne, France*
[3]*Sciences et Ingénierie de la Matière Molle, ESPCI Paris, Université PSL, CNRS, Sorbonne Université, 75005 Paris, France*

Memory effects are a classic feature of disordered materials. With Raman-microspectroscopy we evidence a memory effect in the deformation of densified soda-lime silicate glasses, and with molecular dynamics simulations we identify the network reconfigurations it originates from. These results pave the way toward a better understanding of plastic instability, damage, and rupture properties in iono-covalent glassy materials.

I. PLASTICITY MECHANISMS IN AMORPHOUS SILICATES

In disordered materials, plastic flow is poorly understood. Huge efforts in theory and simulations may soon provide better insight into local scale mechanisms [1–3], but to what extent these concepts apply to real materials is less clear. On the experimental side, notable advances have been registered with granular systems. When samples are made from millimetric grains, structural variables like local density become quite easily measurable [4]. In addition, birefringent pellets can evidence local stress states in 2D systems [5]. Such techniques have been used to probe the relation between structure and plastic response and in particular the memory effects which appear due to the highly nonequilibrium nature of disordered systems [6,7]. A typical experiment is shear reversal where the density distribution in shear bands reveals the connection between local structure and loading history [4,8]. Recently, using x-ray tomography, Xing *et al.* [9] have evidenced an evolution of the network topology under alternating shear in relation to macroscopic loading: such advanced structural studies are necessary to describe the complex response of disordered materials, identify structural indicators of plasticity [3], and build up relevant constitutive models [9,10].

In silicate glasses, plastic deformation is as complex as in granular materials, but even more poorly understood, despite its suspected role in key properties such as damage and fracture [11–16]. Intriguingly, the mechanical properties of a large variety of silicate glasses are all very similar, except their sensitivities to crack initiation which differ widely [17,18]. To resolve this paradox, it has been suggested that it is plastic softening which differentiates these glasses [19,20], further highlighting the need for a better grasp of plastic deformation mechanisms and their relation to structure and rearrangements [16,21]. But in contrast to granular materials and their grain-grain interactions [22], for ionocovalent solids such as silicate glasses, the relevant size for plastic rearrangements is the atomic scale. Adequate experimental tools are scarce especially once two additional constraints have been factored in: disorder and small sample sizes (the plastically deformed areas often extend over tens of microns at most). In this context, Raman microspectroscopy, which has traditionally been used by geophysicists to explore the structure of minerals in diamond anvil cells (DAC) at hydrostatic pressures up to 10 s of GPa [23,24] becomes a useful micromechanics experiment: the stress-strain response of silica glass in the regime of irreversible volumetric deformation (aka densification) has been measured, the Raman spectrum being used as strain gauge [25]. Further derivations of the technique have been applied to other types of loadings namely indentation [26] and uniaxial compression [27]. Such micromechanics experiments have provided a sound experimental basis for the development of constitutive relations for silicates glasses [28,29]. However, they have been mainly applied to fused silica while results for more complex glasses are much less systematic [30,31].

Here, we investigate soda-lime-silicate glasses with Raman microspectroscopy at high pressures and evidence memory effects during hydrostatic loading-unloading cycles. Our results directly point to the existence of specific, plasticity-related metastable structures which we also investigate through molecular dynamics (MD) simulations. Following the structure during loading-unloading cycles, we find evolutions which provide a reasonable explanation for the Raman observations. We also build up an evolution equation to describe the memory effect and discuss the parameter values at the light of the MD results. These results shed direct light on the specific impact of Na on plasticity mechanisms and the presence of metastable states in silicate glasses which pave the way toward a better understanding of the relation between structure, plasticity, local instabilities and damage in materials with atomic scale disorder.

II. HIGH PRESSURE EXPERIMENTS

For silica glass, the evolution of the Raman spectrum with hydrostatic pressure is well known. Local strain under pressure induces a shift of the main band [25]. Up to the yield pressure P_y (10 GPa), this shift reveals a purely elastic regime. Above this pressure, volumetric plastic deformation occurs,
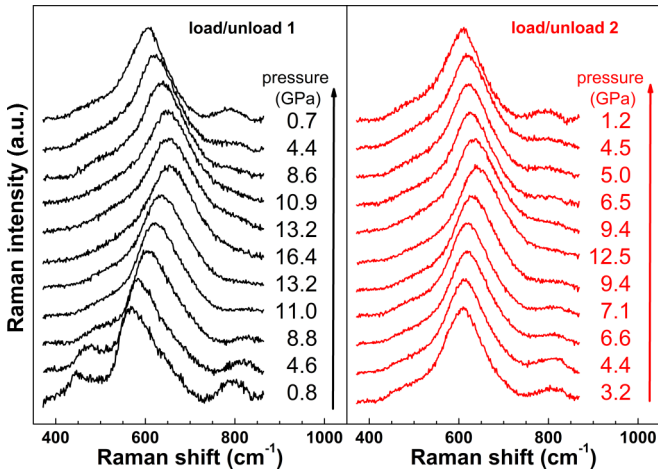
FIG. 1. *In situ* Raman spectra of the soda-lime silicate glass during two successive compression/decompression cycles (first experiment) : $P_{atmo} \rightarrow P_{max}^2 = 16.4$ GPa $\rightarrow P_{atmo}$ (right side, black spectra) and $P_{atmo} \rightarrow P_{max}^3 = 12.5$ GPa $\rightarrow P_{atmo}$ (left side, red spectra).

FIG. 2. Pressure versus Raman shift of the 500–730 cm^{-1} band during pressure cycles (experimental uncertainties given by marker size). The data, from two different experiments with $P_{max} = 12$ GPa (triangles) and 16 GPa (squares) are fitted using the model [Eq. (3)] with (solid red line) and without (dashed blue line) memory effect. Inset—schematics of network structure: (a) below yield pressure, (b) above yield pressure, transition to more homogeneous Na distribution with metastable states (b1–b2) during unloading-loading.

with an irreversible contribution to the shift which increases with the maximum pressure P_{max} experienced by the glass. This pressure P_{max} becomes the new yield pressure so that further unloading-loading at $P < P_{max}$ reveals only an elastic response with no hysteresis. For silicate glasses, even though the glass structure is more complex, the available ex situ Raman data seem to indicate a similar trend. In a previous work, we investigated a soda-lime silicate window glass composed of SiO_2 (72%), Na_2O (15%), CaO (8%), MgO (4%) with Al_2O_3, FeO_3, and SO_3 constituting the remaining 1%. From *ex situ* measurements we determined that the yield pressure is $P_y = 6.5$ GPa and density saturates around 16 GPa [30]. Here we have investigated the Raman signature of the same soda-lime silicate glass in more detail, by performing *in situ* Raman spectroscopy during mechanical deformation (Fig. 1). High-pressure experiments were conducted in a Chervin-type diamond anvil cell. A float glass splinter with a typical size of 30 μm and ruby chips were placed in the metallic gasket hole (200 μm diameter) filled with 4:1 methanol-ethanol mixture as pressure transmitting medium. Successive compression/decompression cycles have been performed and two distinct experiments were made:

(1) First experiment from pristine glass: $P_{atmo} \rightarrow P_{max}^1 = 6, 8$ GPa $\rightarrow P_{atmo} \rightarrow P_{max}^2 = 16.4$ GPa $\rightarrow P_{atmo} \rightarrow P_{max}^3 = 12.5$ GPa $\rightarrow P_{atmo} \rightarrow P_{max}^4 = 12.5$ GPa $\rightarrow P_{atm}$,

(2) Second experiment from pristine glass: $P_{atmo} \rightarrow P_{max}^1 = 11.5$ GPa $\rightarrow P_{atmo} \rightarrow P_{max}^2 = 12.0$ GPa.

The retrieved samples were in one piece, indicating the hydrostatic nature of the pressure cycles. The Raman spectrometer used was a Renishaw RM 1000 microspectrometer equipped with a $50\times$ long working distance objective in backscattering configuration. The excitation line was provided by a Nd^{3+}:YAG crystal laser emitted at 532 nm. Raman spectroscopy was carried out *in situ* during the pressure cycles. Pressures were measured precisely from the ruby R1 band luminescence after each compression or decompression step, with a delay of 10 min before measurement to reach pressure stabilization. 10 min was necessary to record each *in situ*
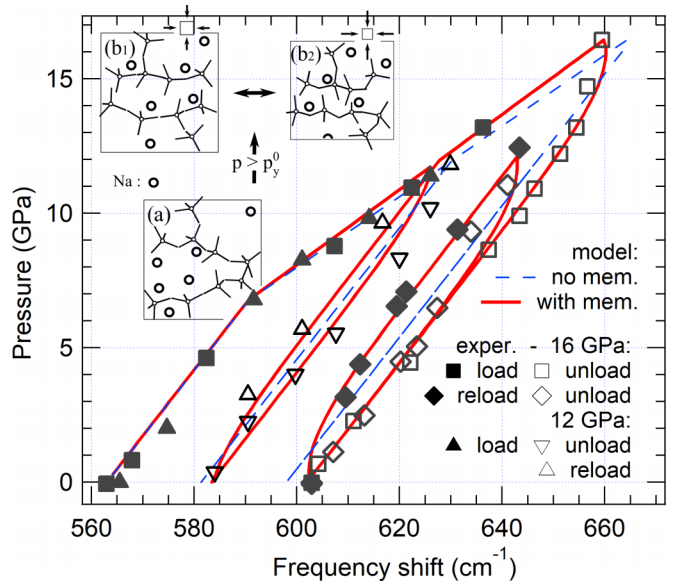
spectrum. The last cycle of the first experiment was dedicated to probe a possible time-dependent relaxation phenomenon of the glass. For this cycle, only two intermediate pressures, at $P = 4.7$ GPa, have been analyzed: one during loading and one during unloading. The sample was monitored at this pressure over 140 h.

In summary, after a first unloading-loading cycle below the elastic limit P_y, we load hydrostatically at a pressure $P_{max} > P_y$ resulting in some densification. Then we apply unloading-loading cycles at pressures $P < P_{max}$. The pressure-dependence of the main band during two of these procedures with $P_{max} = 12$ GPa and 16 GPa is plotted Fig. 2.

The main band shift is reversible for $P_{max} < P_y$ as expected (elastic—not shown). When $P_{max} > P_y$, the material has deformed plastically and the shift during subsequent unloading-loading cycles with $P < P_{max}$ displays hysteresis: upon unloading, the main band lies at a higher frequency than upon loading. If a second unloading is carried out, then there is an accommodation period after which for the same pressure, the same frequency shift is obtained as upon first unloading. We also note that the hysteresis loop for $P_{max} = 12$ GPa has a smaller amplitude than for $P_{max} = 16$ GPa suggesting that the amplitude of the hysteresis cycle increases with plastic strain. We also performed creep measurements over 140 h at $P = 4.7$ GPa during unloading and loading after densification at $P_{max} = 16$ GPa and no time dependence was found, ruling out a viscous contribution. Therefore, we conclude that this hysteresis loop is a memory effect as observed during shear reversal in granular materials for example.
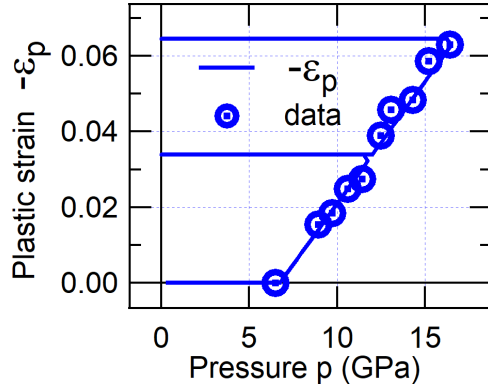
FIG. 3. Volumetric plastic strain as a function of pressure calculated from Eq. (1) along with the data from Ref. [30].

III. PHENOMENOLOGY OF THE MEMORY EFFECT

To model this effect at the continuum lengthscale, we evaluate plastic strain following previous works on float glass [30,32]. The plastic strain itself depends upon stress history and we take a simple hardening rule,

$$\varepsilon_p = -\frac{P_{\max} - P_y^0}{\zeta}, \tag{1}$$

where ζ is the plastic hardening coefficient, $P_{\max}$ the maximum pressure reached during the experiment and P_y^0 the initial yield pressure. For the hardening rule Eq. (1) we use a plastic hardening coefficient $\zeta = 155$ GPa and an initial yield pressure $P_y^0 = 6.5$ GPa (Fig. 3). These plastic deformation parameters are known from previous work on float glass [28,30].

We also introduce an internal variable α to reflect the hysteretic evolution of the material structure and write an equation for the evolution of α with the history of the hydrostatic stress or equivalently of the *elastic* strain $\varepsilon_{el}(t) < 0$. No measurable rate effects have been observed, but because the response depends upon past values, we need to track the variations of the elastic strain ε_{el} through the loading-unloading cycles. The elastic strain itself cannot be used: there is no one-to-one correspondence since it is not monotonic. This is why we use a pseudotime defined by $t = \int d|\varepsilon_{el}|$. It is equal to the elastic strain in the first loading phase but keeps increasing in the unloading phase with $dt = -d\varepsilon_{el}$, etc. (Fig. 4).

Then we can write a generic evolution equation for α involving a memory function such as

$$\alpha(t) = -\varepsilon_p \frac{A}{t_c} \int_0^t f_m\left(\frac{t-\tau}{t_c}\right) \frac{d\varepsilon_{el}}{d\tau} d\tau, \tag{2}$$

For the memory function f_m we take a simple exponential. Two parameters characterize the structural evolution. The amplitude of the memory effect is proportional to the parameter A. It is also proportional to the volumetric plastic strain $\varepsilon_p < 0$ as required by the experimental dependence of the hysteresis amplitude upon $P_{\max}$. This assumption implies that the number of metastable configurations generated by densification is proportional to the plastic strain. The second parameter is the characteristic fictitious time t_c which actually reflects a *characteristic memory strain* ε_c. The evolution of the various model variables for the experimental loading-unloading
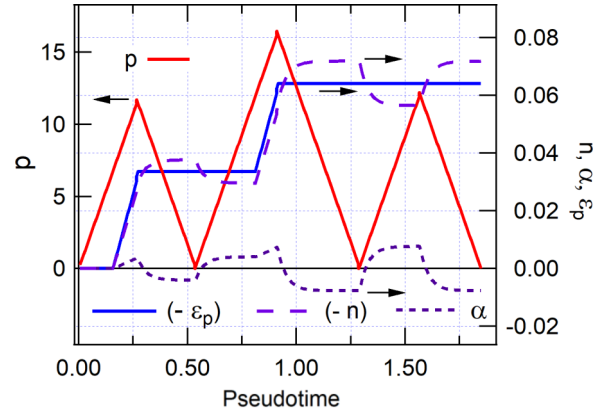

FIG. 4. History of pressure p as a function of pseudotime (defined from elastic strain), densification $-\varepsilon_p$, internal variable α and the spectroscopic variable $-n = -\varepsilon_p - \alpha$

cycles (Fig. 2) are shown in Fig. 4. The exact shape of the memory function is not expected to play a strong role as long as it is monotonically decreasing with integral 1, hence the exponential form.

Finally, we assume that the spectroscopic response ν depends linearly upon elastic strain, plastic strain and internal variable α as

$$\nu = c_0 - c_1[\varepsilon_{el} + c_2(\varepsilon_p + \alpha)] \tag{3}$$

Of these three spectroscopic parameters, two are calibrated from the shift in the elastic regime, giving $c_0 = 563$ cm^{-1} and $c_1 = 175$ cm^{-1} taking the bulk modulus $K = 43$ GPa.

To fit the spectroscopic data during loading-unloading cycles in the plastic region we are left with three parameters A, $\varepsilon_c (= t_c)$ and c_2. The result is shown in Fig. 2 with A = 0.12, $\varepsilon_c = 0.04$ and $c_2 = 3.1$ (solid red line). For comparison the result without hysteresis is also shown (A = 0—dashed blue line). Since α is positive, the shift is reduced for increasing pressure and vice versa. Satisfactory agreement with the data validates the simple assumptions made here for this phenomenological description of the memory effect in the plastically deformed material.

IV. MOLECULAR DYNAMICS SIMULATIONS–STRUCTURAL EVOLUTION DURING VOLUMETRIC FLOW

Beyond this continuum scale description, we have also performed atomic-scale simulations. We use MD simulations to derive insight into possible deformation mechanisms. We aim at a qualitative model which reproduces the phenomenology. These results aim at a better understanding of the physics of plastic deformation in an amorphous silica matrix partly depolymerized by network modifiers. For that purpose, we model a binary sodium silicate glass with 30%mol Na. This simplified composition does not attempt to quantitatively reproduce the response of the material probed experimentally. Such a goal is much more ambitious and would at least require an extensive tuning of the interaction potentials, which is far beyond the scope of the present paper.
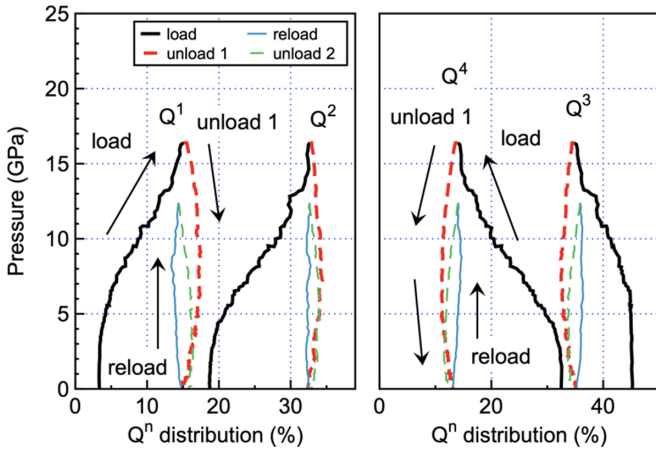
FIG. 5. Silica speciation in MD simulation for $0.3Na_2O$-$0.7SiO_2$ glass as a function of pressure, during two successive pressure cycles with $P_{max} = 16.4$ GPa and 12.4 GPa.
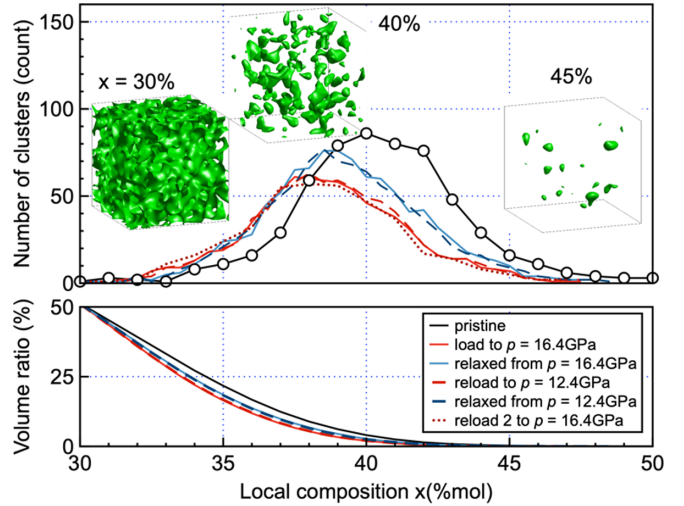

FIG. 6. Na spatial distribution given as number of clusters (top) and relative volume (bottom) as a function of Na density threshold. Results for the pristine material are shown in black, the impact of pressure cycles is shown with blue and red colors.

The interatomic potentials for the sodium silicate were described using the van Beest-Kramer-van Santen (BKS) potential [33] and the parameters set following [34]. The initial samples were first heated at 3000K, then cooled to zero temperature with a cooling rate of 10 K/ps, where quasistatic deformation was performed using a conjugated gradient minimization [35]. To calculate the coordination number of the silicon atoms, the theoretical bond length between Si-O atoms was fixed at $r_{min} = 1.7$ Å: If an O atom had two Si closer than r_{min}, then it was considered bonding (BO). To determine the coordination number of a Si atom, the neighboring BOs were counted. Further technicalities of the MD simulation, its verification and the details of the coarse graining technique can be found in Ref. [35]. To analyze the evolution of the atomic network, the coordination numbers (Q^n with n from 1 to 4) of the Si atoms were determined. The calculated speciation (Fig. 5) shows that during hydrostatic loading, the proportions of Q^3 and Q^4 species in the MD model are first constant then decrease in favour of Q^1 and Q^2 species as pressure exceeds the yield pressure, which is found around 4 to 5 GPa in this model. Clearly, irreversible volumetric deformation results in a less polymerized network. Upon unloading from 16.4 GPa, the speciation stays roughly constant but reloading clearly results in a hysteresis loops: At the same pressure value, the network is more polymerized during loading than unloading. Therefore, the MD simulations corroborate the experimental results and point to structural features which should be connected to the Raman results.

To better understand the structural evolution of the MD system under pressure and its hysteresis, the local composition was calculated based on the coarse grained Na density [35]. Then, to analyze the connectivity of the Na network, we define Na clusters as connected regions in space where the minimal composition is larger than a given composition threshold x (%mol), i.e., the Na density is everywhere larger than x inside the cluster and lower than x immediately outside. In Fig. 6 we plot the number of Na clusters as a function of x: if $x = 30\%$, i.e., the nominal macroscopic composition value, we find one single cluster, which occupies about 50% of the volume of the material. However, certain zones are richer in sodium.

Therefore, if we increase x, then this single cluster splits into several unconnected clusters. For a 40%mol threshold, we find that the number of clusters is maximum and they occupy 5% of the total volume. When pressure is applied to the system (Fig. 6, red), the peak of this cluster number distribution shifts to lower x values, i.e., the higher density clusters disappear (decreasing number but also decreasing volume). Upon unloading, we find that this structural modification is only partly reversible. We conclude that during plastic deformation, sodium atoms tend to migrate from higher density to lower density regions, increasing the number and volume of lower density clusters: volumetric plastic strain homogenises the Na distribution. Furthermore, hysteresis affects this structural evolution during further unloading-loading cycles.

V. DISCUSSION

In fact, a homogenization of the structure through reversible or irreversible densification has been found in previous numerical and experimental observations on silica glass as demonstrated by the distribution of the local rearrangement kinematics [36] and by the size of the elastic heterogeneities evidenced through x-ray scattering [37] or the boson peak [38]. The present MD results suggest that a similar homogenization, shown schematically in Fig. 2 (inset—a to b), exists in silicate glasses with network modifiers. It is effected through local rearrangements of the SiO_2 network around the modifiers, with a variation of the speciation and a depolymerisation of the SiO_2 matrix. We will now connect these results with the observed evolution of the Raman spectra.

In this respect, it is interesting to note that in Eq. (3) the shift parameter for plastic strains c_2 is three times larger than the shift parameter for elastic strains c_1. This disparity in the Raman response attests to the strong change of local environment accompanying irreversible volumetric strain as also evidenced by the evolution of the coordination number

found in the MD simulations. To more directly connect this evolution of the speciation found in MD and the Raman microspectroscopy data, we briefly review the assignment of modes in the main band around $600\,\mathrm{cm}^{-1}$. Xue *et al.* [39] have applied a combination of Raman and NMR on a large range of compositions. Based on their assignments, Deschamps *et al.* [28] have ascribed the main band shift in densified glasses to the dismutation of Q^3 species. More recently, blind deconvolution techniques where applied to extensive composition libraries obtained by evaporation [40] or diffusion [41]. These analyses focused on the so-called Q band around $1100\,\mathrm{cm}^{-1}$. They confirmed that the low frequency range of the Q band is connected to Q^2 species and the high frequency range to Q^4. Applying these hyperspectral analyses to the main band and the Q band simultaneously, Woelffel *et al.* [41] have shown that the converse holds for the main band: it is the high frequency range of the main band which is correlated to the Q^2 species and the low frequency range with the Q^4, in partial agreement with previous literature assignments [30,39]. We conclude that in the plastic regime, the depolymerisation of the network with densification predicted by MD is fully consistent with the shift of the main band to higher frequencies found in the Raman experiments.

To summarize, our results from MD simulations and Raman microspectroscopy show that plastic deformation reduces material heterogeneity and tends to homogenise the distribution of cations. During subsequent elastic unloading-loading cycles, some of those local rearrangements are still active and give rise to hysteresis and the observed memory effect (Fig. 2, inset b1–b2). Therefore, this anelasticity is characterized by back and forth switching between metastable configurations with sufficiently large differences in coordination numbers to be measurable by Raman spectroscopy. In the phenomenological description, the internal variable α actually measures the imbalance between local configurations. At the same applied pressure, a positive α (loading) attests to a more polymerized network and a lower Raman shift. A negative α (unloading) means a less polymerized network and a larger shift. The amplitude A of the hysteresis cycle as determined from the analysis of the Raman data is of the order of 10%: about one tenth of the plastically affected sites actually "switch back and forth" during further elastic unloading-loading cycles [cf Eqs. (2) and (3)]. This fraction is roughly consistent with the fraction of sites affected by the speciation hysteresis in the MD simulations. Similarly, the characteristic memory strain $\varepsilon_c = 0.04$ is also consistent with the value found in MD. Note that in their study of structural indicators, Richard *et al.* [3] observed that the memory of prior strain is fully lost after a strain of about 10% which is consistent with the present value. Of course, even if a change of the average elastic strain of a few percent is enough to flip the small fraction of metastable configurations involved, the local strain fields may be significantly larger than the average value because of the nonaffinity of the local deformation.

Interestingly, the phenomenology of these local configuration rearrangements is reminiscent of internal friction. In a typical experiment, the dynamic small strain response is measured with small amplitude oscillations of a pendulum.

Temperature sweeps well below the glass transition temperature reveal dissipation peaks. For internal friction, these so-called secondary (β) relaxations are due to small amplitude atomic rearrangements with small activation energies, of the order of the thermal energy. Marked effects of internal friction are observed in silicate glasses with a prominent role played by the Na cations, while they are almost absent in silica glass (see Ref. [42] for a review). In our high pressure experiments, however, the memory effect is observed upon relatively large elastic strain (ca 4%). This behavior means that the neighboring configurations are separated by activation energies significantly larger than the thermal energy and configuration switching is only activated by the (local) elastic energy involved in a finite strain macroscopic deformation of the order of ε_c, suggesting that the local plastic instabilities involve a larger number of atoms. Note also that internal friction is observed on the pristine material while we found the memory effect only after initial plastic deformation: the metastable atomic configurations which we detect with Raman appear only with plastic deformation, under the action of high enough pressure. Regarding the connection between local configuration, mechanical response and structural rearrangements, we note that in their review, Richards *et al.* [3] surveyed a large number of structural indicators: some were found to correlate well with local plastic activity while others failed. Interestingly, indicators formed with some measure of the local mechanical response where found to perform better. Vibrational spectroscopy such as Raman is expected to fall in this category. In addition, the structural evolution described here also directly affects the elastodynamic response of the material since similar memory effects can be found in Brillouin spectroscopy for float glass [43] and simple aluminosilicates [44].

VI. CONCLUSION

In summary, we have shown that Raman microspectroscopy can detect metastable configurations leading to memory effects in pre-densified soda-lime-silicate glasses. The initial plastic deformation induces a more out of equilibrium structure but with a more homogeneous Na distribution, as suggested by MD calculations. The concomitant evolution of the speciation is reflected in the Raman shift of the main band. In this modified structure, new metastable configurations appear: ca 10% of the plastic rearrangements can actually switch back and forth during subsequent unloading-loading in the elastic regime, giving rise to hysteresis and memory effect. An average elastic strain of about 10% is large enough to complete most of these transitions. Therefore, in contrast to internal friction, the atomic rearrangements involved are relatively large scale, so that switching involves energy barriers larger than the thermal energy and can be triggered only by sufficient elastic strain. Such spectroscopic signature of a memory effect is a direct footprint of interesting features of the plasticity mechanism in soda-lime silicate glasses. However, it is restricted here to the simplest loading type, namely hydrostatic compression. It is probable that similar rearrangements are operative during shear plasticity, as in granular materials. We expect that the present approach, more difficult to implement in shear in the absence of hardening,

would provide insight into mechanisms critical for material instability such as rearrangement avalanches, formation of shear bands, possibly leading to material rupture. In this respect, the distinct Raman signatures for permanent volumetric strain and permanent shear strain we have demonstrated recently [45] are a very promising cue.

[1] M. L. Falk and J. S. Langer, Deformation and failure of amorphous solidlike materials, Annu. Rev. Condens. Matter Phys. **2**, 353 (2011).

[2] D. Rodney, A. Tanguy, and D. Vandembroucq, Modeling the mechanics of amorphous solids at different length scale and time scale, Model. Simul. Mater. Sci. Eng. **19**, 083001 (2011).

[3] D. Richard, M. Ozawa, S. Patinet, E. Stanifer, B. Shang, S. A. Ridout, B. Xu, G. Zhang, P. K. Morse, J.-L. Barrat *et al.*, Predicting plasticity in disordered solids from structural indicators, Phys. Rev. Materials **4**, 113609 (2020)

[4] B. Utter and R. P. Behringer, Transients in sheared granular matter, Eur. Phys. J. E **14**, 373 (2004).

[5] T. S. Majmudar and R. P. Behringer, Contact force measurements and stress-induced anisotropy in granular materials, Nature (London) **435**, 1079 (2005).

[6] E. M. Bertin, J. P. Bouchaud, J. M. Drouffe, and C. Godreche, The Kovacs effect in model glasses, J. Phys. A **36**, 10701 (2003).

[7] N. C. Keim, J. Hass, B. Kroger, and D. Wieker, Global memory from local hysteresis in an amorphous solid, Phys. Rev. Research **2**, 012004(R) (2020).

[8] M. Toiya, J. Stambaugh, and W. Losert, Transient and Oscillatory Granular Shear Flow, Phys. Rev. Lett. **93**, 088001 (2004).

[9] Y. Xing, J. Zheng, J. Li, Y. Cao, W. Pan, J. Zhang, and Y. Wang, X-Ray Tomography Investigation of Cyclically Sheared Granular Materials, Phys. Rev. Lett. **126**, 048002 (2021).

[10] J. Sun and S. Sundaresan, a constitutive model with microstructure evolution for flow of rate-independent granular materials, J. Fluid Mech. **682**, 590 (2011).

[11] D. M. Marsh, Plastic flow and fracture of glass, Proc. Roy. Soc. A. **279**, 420 (1964).

[12] F. M. Ernsberger, The elastic properties of glasses, in *Elasticity and Strength in Glasses: Glass: Science and Technology*, Vol. 5, edited by D. Uhlmann and N. J. Kreidl (Academic Press, New York, 1980), pp. 1–18.

[13] R. F. Cook and G. M. Pharr, Direct observation and analysis of indentation cracking in glasses and ceramics, J. Am. Ceram. Soc. **73**, 787 (1990).

[14] T. Rouxel and J. C. Sangleboeuf, The brittle to ductile transition in a soda-lime-silica glass, J. Non-Cryst. Solids **271**, 224 (2000).

[15] L. Wondraczek, J. C. Mauro, J. Eckert, U. Kühn, J. Horbach, J. Deubener, and T. Rouxel, Toward ultrastrong glasses, Adv. Mater. **23**, 4578 (2011).

[16] K. Januchta and M. M. Smedskjaer, Indentation deformation in oxide glasses: Quantification, structural changes, and relation to cracking, J. Non-Cryst. Solids X **1**, 100007 (2019).

[17] Y. Kato, H. Yamazaki, S. Yoshida, and J. Matsuoka, Effect of densification on crack initiation under Vickers indentation test, J. Non-Cryst. Solids **356**, 1768 (2010).

[18] P. Sellappan, T. Rouxel, F. Celarie, E. Becker, P. Houizot, and R. Conradt, Composition dependence of indentation deformation and indentation cracking in glass, Acta Mater. **61**, 5949 (2013).

[19] J. T. Hagan, Micromechanics of crack nucleation during indentations, J. Mater. Sci. **14**, 2975 (1979).

[20] E. Barthel, V. Keryvin, G. Rosales-Sosa, and G. Kermouche, Indentation cracking in silicate glasses is directed by shear flow, not by densification, Acta Mater. **194**, 473 (2020).

[21] A. K. Varshneya, Stronger glass products: Lessons learned and yet to be learned, Int. J. App. Glass Sci. **9**, 140 (2018).

[22] B. Kou, Y. Cao, J. Li, C. Xia, Z. Li, H. Dong, A. Zhang, J. Zhang, W. Kob, and Y. Wang, Granular materials flow like complex fluids, Nature (London) **551**, 360 (2017).

[23] C. Meade and R. Jeanloz, Yield strength of MgO to 40 GPa, J. Geophys. Res. **93**, 3261 (1988).

[24] A. Polian and M. Grimsditch, Room-temperature densification of a-SiO$_2$ versus pressure, Phys. Rev. B **41**, 6086 (1990).

[25] D. Vandembroucq, T. Deschamps, C. Coussa, A. Perriot, E. Barthel, B. Champagnon, and C. Martinet, Density hardening plasticity and mechanical aging of silica glass under pressure: A Raman spectroscopic study, J. Phys.: Condens. Matter **20**, 485221 (2008).

[26] A. Perriot, D. Vandembroucq, E. Barthel, V. Martinez, L. Grosvalet, C. Martinet, and B. Champagnon, Raman microspectroscopic characterization of amorphous silica plastic behavior, J. Am. Ceram. Soc. **89**, 596 (2006).

[27] R. Lacroix, G. Kermouche, J. Teisseire, and E. Barthel, Plastic deformation and residual stresses in amorphous silica pillars under uniaxial loading, Acta Mater. **60**, 5555 (2012).

[28] G. Kermouche, E. Barthel, D. Vandembroucq, and Ph. Dubujet, Mechanical modelling of indentation-induced densification in amorphous silica, Acta Mater. **56**, 3222 (2008).

[29] G. Molnar, P. Ganster, J. Török, and A. Tanguy, Sodium effect on static mechanical behavior of MD-modeled sodium silicate glasses, J. Non-Cryst. Solids **440**, 12 (2016).

[30] T. Deschamps, C. Martinet, C. J. L. Bruneel, and B. Champagnon, Soda-lime silicate glass under hydrostatic pressure and indentation: A micro-Raman study, J. Phys.: Condens. Matter **23**, 035402 (2011).

[31] R. Limbach, A. Winterstein-Beckmann, J. Dellith, D. Möncke, and L. Wondraczek, Plasticity, crack initiation and defect resistance in alkali-borosilicate glasses: From normal to anomalous behavior, J. Non-Cryst. Solids **417**, 15 (2015).

[32] T. Rouxel, H. Ji, T. Hammouda, and A. Moreac, Poisson's Ratio and the Densification of Glass Under High Pressure, Phys. Rev. Lett. **100**, 225501 (2008).

[33] B. W. Van Beest, G. J. Kramer, and R. A. Van Santen, Force Fields for Silicas and Aluminophosphates Based on *ab initio* Calculations, Phys. Rev. Lett. **64**, 1955 (1990).

[34] X. Yuan and A. N. Cormack, Local structures of MD-modeled vitreous silica and sodium silicate glasses, J. Non-Cryst. Solids **283**, 69 (2001).

[35] G. Molnar, P. Ganster, and A. Tanguy, Effect of composition and pressure on the shear strength of sodium silicate glasses: An atomic scale simulation study, Phys. Rev. E **95**, 043001 (2017).

[36] B. Mantisi, G. Kermouche, E. Barthel, and A. Tanguy, Impact of pressure on plastic yield in amorphous solids with open structure, Phys. Rev. E **93**, 033001 (2016).

[37] G. Baldi, M. Zanatta, E. Gilioli, V. Milman, K. Refson, B. Wehinger B. Winkler, A. Fontana, and G. Monaco, Emergence of Crystal-Like Atomic Dynamics in Glasses at the Nanometer Scale, Phys. Rev. Lett. **110**, 185503 (2013).

[38] T. Deschamps, C. Martinet, D. R. Neuville, D. de Ligny, C. Coussa-Simon, and B. Champagnon, Silica under hydrostatic pressure: A non-continuous medium behaviour, J. Non-Cryst. Solids **355**, 2422 (2009).

[39] X. Xue, J. F. Stebbins, M. Kanzaki, P. F. McMillan, and B. Poe, Pressure-induced silicon coordination and tetrahedral structural changes in alkali oxide-silica melts up to 12 GPa: NMR, Raman, and infrared spectroscopy, Am. Miner. **76**, 8 (1991).

[40] V. P. Zakaznova-Herzog, W. J. Malfait, F. Herzog, and W. E. Halter, Quantitative Raman spectroscopy: Principles and application to potassium silicate glasses, J. Non-Cryst. Solids **353**, 4015 (2007).

[41] W. Woelffel, C. Claireaux, M. J. Toplis, E. Burov, E. Barthel, A. Shukla, J. Biscaras, M.-H. Chopinet, and E. Gouillard, Analysis of soda-lime glasses using non-negative matrix factor deconvolution of raman spectra, J. Non-Cryst. Solids **428**, 121 (2015).

[42] W. A. Zdaniewski, G. E. Rindone, and D. E. Day, The internal friction of glasses, J. Mater. Sci. **14**, 763 (1979).

[43] S. N. Tkachev, M. H. Manghnani, and Q. Williams, *In situ* Brillouin Spectroscopy of a Pressure-Induced Apparent Second-Order Transition in a Silicate Glass, Phys. Rev. Lett. **95**, 057402 (2005).

[44] C. Sonneville, D. de Ligny, A. Mermet, B. Champagnon, C. Martinet, G. H. Henderson, T. Deschamps, J. Margueritat, and E. Barthel, *In situ* Brillouin study of sodium alumino silicate glasses under pressure, J. Chem. Phys. **139**, 074501 (2013).

[45] C. Martinet, M. Heili, V. Martinez, G. Kermouche, G. Molnar, N. Shcheblanov, E. Barthel, and A. Tanguy, Highlighting the impact of shear strain on the SiO_2 glass structure: From experiments to atomistic simulations, J. Non-Cryst. Solids **533**, 119898 (2020).